

RECURRENT OUTBURSTS REVEALED IN 3XMM J031820.8-663034

HAI-HUI ZHAO¹, SHAN-SHAN WENG¹, JUN-XIAN WANG^{2,3}

¹ Department of Physics and Institute of Theoretical Physics, Nanjing Normal University, Nanjing 210023, China

² CAS Key Laboratory for Research in Galaxies and Cosmology, Department of Astronomy, University of Science and Technology of China, Hefei 230026, China and

³ School of Astronomy and Space Science, University of Science and Technology of China, Hefei 230026, China

Draft version August 2, 2021

ABSTRACT

3XMM J031820.8-663034, first detected by *ROSAT* in NGC 1313, is one of a few known transient ultraluminous X-ray sources (ULXs). In this paper, we present decades of X-ray data of this source from *ROSAT*, *XMM-Newton*, *Chandra* and the Neil Gehrels *Swift* Observatory. We find that its X-ray emission experienced four outbursts since 1992, with a typical recurrent time ~ 1800 days, an outburst duration $\sim 240 - 300$ days, and a nearly constant peak X-ray luminosity $\sim 1.5 \times 10^{39}$ erg/s. The upper limit of X-ray luminosity at the quiescent state is $\sim 5.6 \times 10^{36}$ erg/s, and the total energy radiated during one outburst is $\sim 10^{46}$ erg. The spectra at the high luminosity states can be described with an absorbed disk black-body, and the disk temperature increases with the X-ray luminosity. We compare its outburst properties with other known transient ULXs including ESO 243-49 HLX-1. As its peak luminosity only marginally puts it in the category of ULXs, we also compare it with normal transient black hole binaries. Our results suggest that the source is powered by an accreting massive stellar-mass black hole, and the outbursts are triggered by the thermal-viscous instability.

Keywords: accretion, accretion disks — black hole physics — X-rays: binaries — X-rays: stars — X-rays: individual (3XMM J031820.8-663034)

1. INTRODUCTION

Galactic low-mass X-ray binaries (LMXBs) span most their time in quiescence and enter into outbursts occasionally with X-ray luminosity increased by several orders of magnitude (e.g. Chen et al. 1997; Corral-Santana et al. 2016). Black hole LMXBs manifest themselves into five well-known spectral states (see Fender et al. 2004; McClintock & Remillard 2006; Zhang 2013; Yuan & Narayan 2014, for reviews). As luminosity increases, sources leave the “off” state (i.e. the quiescent state, $L_X < 10^{34}$ erg/s), and enter the low/hard state and the high/soft state. The X-ray spectra at the low/hard and the quiescent states are dominated by a power-law component. In contrast, the high/soft state is dominated by thermal emission from the accretion disk with much weaker variabilities. Meanwhile, the very high state and the intermediate state, representing transitions between the low/hard state and the high/soft state (e.g. McClintock & Remillard 2006), have more complex spectral and temporal behaviors. Additionally, a few rare LMXBs could show episodes of super-Eddington accretion, e.g. V4641 Sgr (Revnivtsev et al. 2002) and V404 Cyg (e.g. Motta et al. 2017). The behaviors become sophisticated in these outbursts, and the knowledge on them is rather rudimentary.

It is widely accepted that outbursts of LMXBs result from thermal-viscous instability in accretion disk (e.g. Chen et al. 1997; Dubus et al. 2001). When the mass transfer rate from the donor star onto the compact object is less than a critical value, the inner region of the accretion disk is hot while the temperature of the outer disk drops below 6000 K – somewhere in between the disk

should hence be unstable. This is because the accretion material in this region is partially ionized, and the hydrogen recombination results in a large change in opacity. Consequently, this region could be out of thermal-viscous equilibrium, and the instability would propagate in the disk, triggering an outburst. It has been noticed that such standard disk instability model (DIM) fails to explain some observed properties of the outbursts (e.g. the typical “fast-rise exponential-decay” light curves), and additional irradiation and truncation disk effects should be taken into account (see Lasota 2001, for reviews).

Compared to LMXBs, ultraluminous X-ray sources (ULXs) found in nearby galaxies are more powerful ($L_X > 10^{39}$ erg/s) and more stable in X-ray (see Feng & Soria 2011; Kaaret et al. 2017, for reviews). In general, the X-ray luminosities of ULXs vary by a factor of ≤ 10 . For instance, M33 X-8 exhibits an X-ray variation amplitude of $< 50\%$ since discovered in 1981 (Weng et al. 2009; La Parola et al. 2015). Since their temporal and spectral properties are quite different from those observed in LMXBs, most ULXs are suggested as massive stellar-mass black holes (MsBHs, $M_{\text{BH}} \sim 20 - 100 M_{\odot}$) with super-Eddington accretion (Feng & Soria 2011; Weng et al. 2014). In such a system, the mass transfer rate is large enough to keep the whole disk fully ionized (with the aid of powerful irradiation), and therefore the accretion proceeds stably.

However, a number of ULXs show more dramatic luminosity variations, manifesting themselves as transients (e.g. Zezas et al. 2006; Grimm et al. 2007; Crivellari et al. 2009). These sources may provide a bridge between LMXBs and luminosity ULXs. Due to the lack of observations, only a few transient ULXs have been studied in detail (e.g. Kaur et al. 2012; Middleton et al. 2012). It is yet unclear whether the out-

bursts in transient ULXs are driven by the DIM.

3XMM J031820.8-663034 (R.A. = 03:18:20.8, Dec = -66:30:35) is $0.8'$ away from the center of NGC 1313. It was first detected by *ROSAT* with a maximum X-ray luminosity of $L_X \sim 1.2 \times 10^{39}$ erg/s (Liu & Bregman 2005) by assuming a distance of $d = 4.61$ Mpc (Gao et al. 2015). Investigating a set of *XMM-Newton* data, Lin et al. (2014) found that the source was only detected in two out of fourteen observations, revealing a transient nature of this source. Because there are two persistent ULXs (i.e. NGC 1313 X-1 and NGC 1313 X-2, Petre et al. 1994; Makishima et al. 2000; Bachetti et al. 2013; Weng et al. 2014; Pinto et al. 2016; Kosec et al. 2018), and one bright supernova (SN 1978K, Ryder et al. 1993; Zhao et al. 2017) in this region, numerous X-ray observations have been devoted to explore the spectral evolution of these sources. In this paper, we analyze all available X-ray data of 3XMM J031820.8-663034, collected by *ROSAT*, *Chandra*, *XMM-Newton*, and the Neil Gehrels *Swift* Observatory, and report its recurrent activities. The data reduction and results are described in §2. Because its peak luminosity marginally puts it in the category of ULXs, we compare in §3 its outburst properties with those of both known transient ULXs and normal LMXBs. We also discuss the origin of the outbursts and determine the black hole mass in 3XMM J031820.8-663034 according to the spectral investigation (§3).

2. DATA REDUCTION & RESULTS

2.1. *XMM-Newton* data

A total of 21 *XMM-Newton* observation covering 3XMM J031820.8-663034 were made from 2000 October and 2016 March (Table 1). We reduce all data collected from the EPIC camera (Strüder et al. 2001; Turner et al. 2001) using the Science Analysis System software (SAS) version 14.0.0¹, and the intervals contaminated by flaring particle background are discarded. Besides the detections during two observations reported in Lin et al. (2014), the source turned up on MJD 56844 again. For the first two observations, only the EPIC-pn data are analyzed because the source fell in CCD gaps of MOS1/MOS2. Due to the same reason, we only use MOS1/MOS2 data for the observation on MJD 56844. Circular regions with radii of $15''$ and $30''$ are adopted for the source and background (nearby source free region), respectively. The spectral response files are generated by the SAS task `rmfgen` and `arfgen`, and the spectra are grouped to have at least 15 counts per bin with the task `specgroup` to enable the use of chi-square statistics.

Both an absorbed steep power-law ($\Gamma \sim 2.2 - 2.5$) and a disk black-body (`tbabs*diskbb` in XSPEC, Arnaud 1996) provide adequate fits to the first two observations (Figure 1 and Table 2). The derived parameters are consistent with those reported by Lin et al. (2014, Table 3 in their paper). The spectrum obtained on MJD 56844, however, is poorly fitted by an absorbed power-law ($\chi^2_\nu/dof \sim 1.68$, Table 2 and Figure 1), corresponding to a null hypothesis probability of 1.2×10^{-6} . Contrarily, the data can be well described by a disk black-body ($\chi^2_\nu \sim 1.10$), and an additional power-law compo-

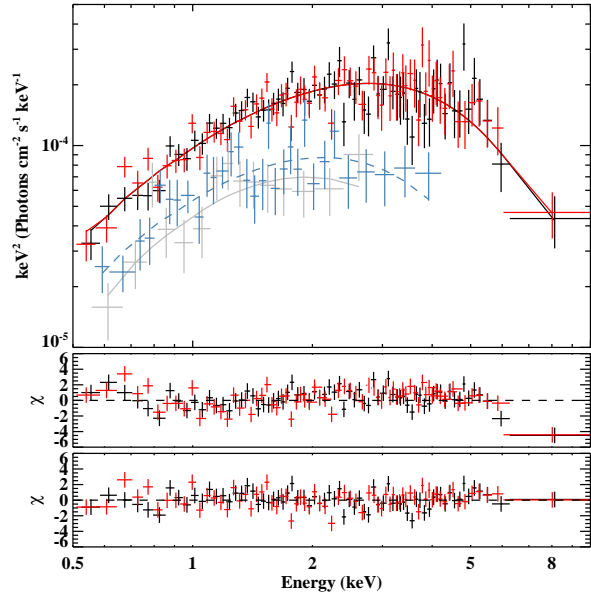


Figure 1. Upper panel: *XMM-Newton* MOS1 (black) and MOS2 (red) spectra observed on 2014 July 5-6 (ObsID = 0742590301), and the best-fit absorbed *diskbb* model. Middle and Lower panels: the fitting residuals to an absorbed powerlaw model and an absorbed *diskbb* model, respectively. The *XMM pn* spectra observed on MJD 53332 and 53408 are also plotted in the upper panel (grey and light-blue) for comparison.

nent is statistically not required ($< 99\%$ according to *F-test*). As shown in Figure 2, the disk temperature (kT) increases with the unabsorbed X-ray luminosity in 0.5–10 keV. We fit the $L_X - kT$ relation with a power-law function and take the error of kT into account. The best fitted power-law index $n = 2.9 \pm 1.3$ is roughly consistent with $L_X \propto kT^4$ (as predicted by the standard disk model with a constant inner radius, i.e. the innermost stable circular orbit).

3XMM J031820.8-663034 was not detected in the other 18 *XMM-Newton* observations, and 2σ upper limits to the source count rates are estimated with the SAS task `eregionanalyse` (Table 1).

2.2. *Swift* observations

In this work, we analyze all 371 *Swift* (Gehrels et al. 2004) observations made before 2017 July. Two episodic outbursts of 3XMM J031820.8-663034 have been caught by the *Swift* dense observations, and *Swift* monitored the second entire outburst (Figure 3). The exposure time of individual *Swift* observations ranges from 138 s to 7.75 ks, with a mean value of 1.3 ks. We extract the source counts in 0.3–10 keV band from a circle aperture with a radius of 6 pixels centered at the source position, and the background from nearby source free regions. The telescope vignetting and point spread function corrections are applied by running the *Swift* script `xrtlccorr`.

Due to the limited photons in individual pointings, we stack all observations during each of the two outbursts. As only 137 photon counts were collected during the outburst in MJD 55050–55200, we rebin the spectrum to have at least 5 counts per bin and employ the C-statistic (Cash 1979) in spectral fitting. During the 2nd outburst, a total of 396 counts were detected. We group

¹ <https://heasarc.gsfc.nasa.gov/docs/xmm/abc/>

Table 1
X-ray observations log

Instrument	ObsID	Date	MJD	Energy (keV)	Net exposure (ks)	Count rate (cts s ⁻¹)	Flux (erg cm ⁻² s ⁻¹)
<i>XMM-Newton</i> /pn ^M	0106860101	2000-10-17	51834	0.5–10	22.3	< 3.0 × 10 ⁻³	< 1.0 × 10 ⁻¹⁴
<i>XMM-Newton</i> /pn ^T	0150280101	2003-11-25	52968	0.5–10	1.2	< 1.1 × 10 ⁻²	< 3.8 × 10 ⁻¹⁴
<i>XMM-Newton</i> /pn ^T	0150280301	2003-12-21	52994	0.5–10	8.6	< 4.1 × 10 ⁻³	< 1.4 × 10 ⁻¹⁴
<i>XMM-Newton</i> /pn ^T	0150280401	2003-12-23	52996	0.5–10	4.1	< 3.8 × 10 ⁻³	< 1.3 × 10 ⁻¹⁴
<i>XMM-Newton</i> /pn ^T	0150280501	2003-12-25	52998	0.5–10	6.0	< 8.5 × 10 ⁻³	< 2.9 × 10 ⁻¹⁴
<i>XMM-Newton</i> /pn ^T	0150280601	2004-01-08	53012	0.5–10	10.2	< 4.1 × 10 ⁻³	< 1.4 × 10 ⁻¹⁴
<i>XMM-Newton</i> /pn ^T	0150281101	2004-01-16	53020	0.5–10	5.9	< 6.1 × 10 ⁻³	< 2.1 × 10 ⁻¹⁴
<i>XMM-Newton</i> /pn ^T	0205230201	2004-05-01	53126	0.5–10	0.7	< 1.0 × 10 ⁻²	< 3.5 × 10 ⁻¹⁴
<i>XMM-Newton</i> /pn ^T	0205230301	2004-06-05	53161	0.5–10	10.0	< 6.7 × 10 ⁻³	< 2.2 × 10 ⁻¹⁴
<i>XMM-Newton</i> /pn ^T	0205230401	2004-08-23	53240	0.5–10	10.1	< 4.4 × 10 ⁻³	< 1.4 × 10 ⁻¹⁴
<i>XMM-Newton</i> /pn ^T	0205230501	2004-11-23	53332	0.5–10	12.5	(2.2 ± 0.1) × 10 ⁻²	(2.0 ^{+0.8} _{-0.4}) × 10 ⁻¹³
<i>XMM-Newton</i> /pn ^T	0205230601	2005-02-07	53408	0.5–10	9.8	(6.2 ± 0.2) × 10 ⁻²	(2.5 ^{+0.3} _{-0.3}) × 10 ⁻¹³
<i>XMM-Newton</i> /pn ^M	0301860101	2006-03-06	53800	0.5–10	19.9	< 8.5 × 10 ⁻³	< 2.9 × 10 ⁻¹⁴
<i>XMM-Newton</i> /pn ^M	0405090101	2006-10-15	54023	0.5–10	98.8	< 4.3 × 10 ⁻³	< 1.5 × 10 ⁻¹⁴
<i>XMM-Newton</i> /pn ^M	0693850501	2012-12-16	56277	0.5–10	110.7	< 6.3 × 10 ⁻³	< 2.1 × 10 ⁻¹⁴
<i>XMM-Newton</i> /pn ^M	0693851201	2012-12-22	56283	0.5–10	114.8	< 6.2 × 10 ⁻³	< 2.1 × 10 ⁻¹⁴
<i>XMM-Newton</i> /pn ^M	0722650101	2013-06-08	56451	0.5–10	22.3	< 5.3 × 10 ⁻³	< 1.8 × 10 ⁻¹⁴
<i>XMM-Newton</i> /MOS ^M	0742590301	2014-07-05	56844	0.5–10	61.0/61.0	(4.7 ± 0.1) × 10 ⁻²	(5.9 ^{+0.2} _{-0.2}) × 10 ⁻¹³
<i>XMM-Newton</i> /pn ^M	0742490101	2015-03-30	57111	0.5–10	94.8	< 4.2 × 10 ⁻³	< 1.4 × 10 ⁻¹⁴
<i>XMM-Newton</i> /pn ^T	0764770101	2015-12-05	57361	0.5–10	65.3	< 3.2 × 10 ⁻³	< 1.1 × 10 ⁻¹⁴
<i>XMM-Newton</i> /pn ^T	0764770401	2016-03-23	57470	0.5–10	21.9	< 3.4 × 10 ⁻³	< 1.2 × 10 ⁻¹⁴
<i>Swift</i> /XRT	...	Quiescence*	...	0.3–10	365	< 2.6 × 10 ⁻⁴	< 1.1 × 10 ⁻¹⁴
<i>ROSAT</i> /PSPC	rp600045n00	1991-04-24	48371	0.1–2.5	11.0	< 4.9 × 10 ⁻⁴	< 1.7 × 10 ⁻¹⁴
<i>ROSAT</i> /HRI	rh400065n00	1992-04-18	48730	0.1–2.5	5.4	< 1.1 × 10 ⁻³	< 1.0 × 10 ⁻¹³
<i>ROSAT</i> /PSPC	rp600504n00	1993-11-03	49294	0.1–2.5	15.2	< 2.5 × 10 ⁻⁴	< 8.1 × 10 ⁻¹⁵
<i>ROSAT</i> /HRI	rh600505n00	1994-06-23	49527	0.1–2.5	22.6	(5.63 ± 0.66) × 10 ⁻³	5.3 × 10 ⁻¹³
<i>ROSAT</i> /HRI	rh500403n00	1995-01-31	49748	0.1–2.5	13.6	< 2.2 × 10 ⁻³	< 2.1 × 10 ⁻¹³
<i>ROSAT</i> /HRI	rh500404n00	1995-02-02	49750	0.1–2.5	27.4	(1.60 ± 0.36) × 10 ⁻³	1.5 × 10 ⁻¹³
<i>ROSAT</i> /HRI	rh600505a01	1995-04-12	49819	0.1–2.5	20.4	< 2.3 × 10 ⁻³	< 2.2 × 10 ⁻¹³
<i>ROSAT</i> /HRI	rh500404a01	1995-05-08	49845	0.1–2.5	19.1	< 1.0 × 10 ⁻³	< 9.4 × 10 ⁻¹⁴
<i>ROSAT</i> /HRI	rh500403a01	1995-05-09	49846	0.1–2.5	31.4	< 6.5 × 10 ⁻⁴	< 6.1 × 10 ⁻¹⁴
<i>ROSAT</i> /HRI	rh500492n00	1997-09-30	50721	0.1–2.5	23.0	< 8.9 × 10 ⁻⁴	< 8.4 × 10 ⁻¹⁴
<i>ROSAT</i> /HRI	rh500550n00	1998-03-21	50893	0.1–2.5	24.2	< 6.2 × 10 ⁻⁴	< 5.8 × 10 ⁻¹⁴
<i>Chandra</i> /HRC-I	2935	2002-09-19	52536	0.08–10	1.8	< 1.8 × 10 ⁻³	< 4.4 × 10 ⁻¹⁴
<i>Chandra</i> /ACIS-S	2950	2002-10-13	52560	0.5–7	19.9	< 2.3 × 10 ⁻⁴	< 2.2 × 10 ⁻¹⁵
<i>Chandra</i> /ACIS-I	3550	2002-11-09	52587	0.5–7	14.6	< 5.2 × 10 ⁻⁴	< 8.4 × 10 ⁻¹⁵
<i>Chandra</i> /ACIS-I	3551	2003-10-02	52914	0.5–7	14.8	< 2.1 × 10 ⁻⁴	< 3.2 × 10 ⁻¹⁵
<i>Chandra</i> /ACIS-S	4747	2003-11-17	52960	0.5–7	5.3	< 7.5 × 10 ⁻⁴	< 7.0 × 10 ⁻¹⁵
<i>Chandra</i> /ACIS-S	4748	2004-02-22	53057	0.5–7	5.1	< 6.1 × 10 ⁻⁴	< 5.9 × 10 ⁻¹⁵
<i>Chandra</i> /ACIS-S	4750	2004-02-22	53057	0.5–7	4.7	< 6.6 × 10 ⁻⁴	< 6.9 × 10 ⁻¹⁵
<i>Chandra</i> /ACIS-I	14676	2012-12-17	56278	0.5–7	9.8	< 4.6 × 10 ⁻⁴	< 8.2 × 10 ⁻¹⁵
<i>Chandra</i> /ACIS-I	15594	2012-12-24	56285	0.5–7	9.8	< 3.1 × 10 ⁻⁴	< 5.5 × 10 ⁻¹⁵

Note. — Energy: Energy band used to estimate the photon counts from each instrument. pn^M: Medium filter was used. pn^T: Thin filter was used. Quiescence: The summed image in 0.3–10 keV is generated for all *Swift*/XRT in the quiescence state (see text). Count rate: The 95.45% confidence upper limit in the corresponding energy band is given when the source is undetected. Flux: The unabsorbed flux (or its 2σ upper limit) in 0.5–10 keV is estimated by assuming a power-law model ($nH = 6 \times 10^{20}$ cm⁻² and $\Gamma = 1.7$).

Table 2
Spectral fitting results

Observatory	MJD	nH (10 ²¹ cm ⁻²)	Γ	χ^2/dof	nH (10 ²¹ cm ⁻²)	kT (keV)	$Norm$ (×10 ⁻³)	χ^2/dof	Flux
<i>XMM-Newton</i>	53332	2.5 ^{+2.3} _{-1.9}	2.2 ^{+1.0} _{-0.8}	9.8/12	0.9 ^{+1.4}	0.77 ^{+0.65} _{-0.24}	30.0 ^{+140.9}	11.0/12	2.0 ^{+0.8} _{-0.4}
<i>XMM-Newton</i>	53408	2.7 ^{+1.1} _{-1.0}	2.4 ^{+0.4} _{-0.4}	21.3/28	0.6 ^{+0.6}	0.88 ^{+0.19} _{-0.15}	22.4 ^{+26.2} _{-12.1}	25.1/28	2.5 ^{+0.3} _{-0.3}
<i>XMM-Newton</i>	56844	3.3 ^{+0.3} _{-0.3}	2.3 ^{+0.1} _{-0.1}	229.7/137	0.5 ^{+0.1} _{-0.1}	1.16 ^{+0.05} _{-0.05}	17.1 ^{+3.0} _{-2.4}	151.4/137	5.9 ^{+0.2} _{-0.2}
<i>Swift</i>	55050–55200 [‡]	2.2 ^{+2.2} _{-1.9}	2.0 ^{+0.6} _{-0.5}	19.2/22	0.3 ^{+1.5}	1.2 ^{+0.4} _{-0.3}	4.9 ^{+10.5}	18.7/22	2.0 ^{+0.5} _{-0.4}
<i>Swift</i>	56800–57100	3.8 ^{+1.5} _{-1.2}	2.4 ^{+0.4} _{-0.3}	16.5/22	1.3 ^{+0.9} _{-0.8}	0.9 ^{+0.2} _{-0.1}	17.4 ^{+18.6} _{-8.9}	15.3/22	2.3 ^{+0.3} _{-0.3}

Note. — Flux: 0.5–10.0 keV absorbed flux calculated with the disk black-body model in units of 10⁻¹³ erg cm⁻² s⁻¹. All errors are in the 90% confidence level (1.645σ). ‡: The C-statistic is adopted for the spectral fitting.

the spectrum to have at least 15 counts per bin and the common χ^2 statistic is applied. The spectral modeling confirms that the X-ray spectra during the outbursts are very soft, and can be fitted by either an absorbed steep power-law ($\Gamma \sim 2 - 2.4$) or a disk black-body (Table 2). During other *Swift* observations, 3XMM J031820.8-663034 remains undetected. We estimate an upper limit of count rate $\sim 2.6 \times 10^{-4}$ cts/s (or an upper limit of $L_X \sim 2.8 \times 10^{37}$ erg/s) by summing all observations in the off state (with total exposure of ~ 365 ks from 285 snapshots).

As shown explicitly in Figure 3, 3XMM J031820.8-663034 has almost the same peak luminosity during two outbursts. Coincidentally, when the source reached the peak of the second outburst, the *XMM-Newton* observation recorded an X-ray luminosity of $L_X \sim 1.5 \times 10^{39}$ erg/s (Section 1). Using the *XMM-Newton* spectral fitting model, we convert count rates (and upper limits) from different instruments into those expected from *Swift*/XRT, and plot them in Figures 3 and 4 for comparison.

2.3. ROSAT and Chandra archival data

We employ the XIMAGE software to measure the count rate in all 9 *ROSAT*/HRI and 2 *ROSAT*/PSPC images (Truemper 1982; Pfeffermann et al. 1987). 3XMM J031820.8-663034 was detected in 2 images ($> 2\sigma$), and a maximum count rate (5.63×10^{-3} cts/s) was obtained on MJD 49527 (see Table 1). Assuming a power-law with photon index of 1.7, we run the tool WebPIMMS² and estimate an unabsorbed luminosity of $\sim 1.3 \times 10^{39}$ erg/s (0.5 – 10 keV), which is consistent with the value reported in Liu & Bregman (2005).

From September, 2002 to December, 2012, *Chandra* (Weisskopf et al. 2000) visited the source region 9 times. However, the 3XMM J031820.8-663034 was in quiescence state and was not detected in any observation. We estimate the flux upper limit with the tasks `srcflux/aprates`³ in the CIAO⁴ software (version 4.6.7). The deepest observation (ObsID = 2950) yields the strongest upper limit to its X-ray luminosity ($\sim 5.6 \times 10^{36}$ erg/s), which is more than two orders of magnitude fainter comparing with its maximum luminosity during the outbursts.

2.4. Outburst parameters

The *Swift* monitored the entire outburst from MJD ~ 56800 to 57100, suggesting a fast rise slow decay light curve profile, an outburst duration of $\sim 240 - 300$ days and a total energy radiated during the outburst of $\sim 10^{46}$ erg/s. However, we are unable to determine the light curve profile precisely, including the rise and decay timescales owing to the large uncertainties of *Swift* data. The maximum fluxes recorded in *ROSAT*, *Swift*, and *XMM-Newton* data indicate that the peak luminosity remains constant ($\sim 1.5 \times 10^{39}$ erg/s) during different outbursts. The strongest upper limit for the quiescence state comes from the deepest *Chandra* pointing, indicating a variation amplitude of > 270 .

² <https://heasarc.gsfc.nasa.gov/cgi-bin/Tools/w3pimms/w3pimms.pl>

³ <http://cxc.harvard.edu/ciao/threads/upperlimit/>

⁴ <http://asc.harvard.edu/ciao/>

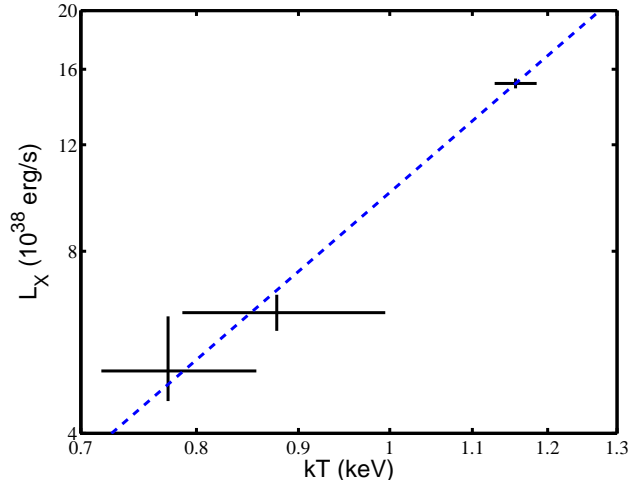


Figure 2. The unabsorbed X-ray luminosity in the 0.5–10 keV band vs. disk temperature with their 1σ errors. The blue dashed line indicates the best-fit $L_X \propto kT^n$ relation with $n = 2.9 \pm 1.3$.

We plot X-ray count rates (and upper limits) from all observations in Fig. 4. All count rates from instruments other than *Swift*/XRT are converted into (with WebPIMMS) XRT count rates for comparison. For three XMM detections, the best-fit spectral models were adopted for the conversion. For *ROSAT* observations and all other upper limits, as accurate spectral modeling is unavailable, we assume a typical low/hard state spectrum for conversion, i.e. a hard power-law model ($nH = 6 \times 10^{20}$ cm⁻² and $\Gamma = 1.7$).

It seems that the source enters into outburst regularly with a recurrent time of ~ 1800 days. We calculate the Lomb-Scargle periodogram (Horne & Baliunas 1986) in a timescale range from 10 days to 5000 days with 50,000 independent frequencies. Since the source was non-detected during most observations, omitting these non-detections would yield too sparse sampling, and no periodical signal emerges in the periodogram. Here, we take all data into account, and 2σ upper limits to the count rates are adopted for those non-detections. As can be seen in Figure 5, the signal at ~ 1750 days and its 2nd/3rd harmonic frequencies ($P \sim 815/580$ days) are higher than 99.9% white noise confidence level. Because the structured window function might lead to aliasing of signals in the data (e.g. VanderPlas 2017), we examine the window power spectrum and do not find any significant feature. We further model the periodogram in the range of 1500-2000 days with a Gaussian, yielding a best-fit period of 1744 days with a FWHM of ~ 418 days. The recurrent time of ~ 1800 days is also verified with the folded light curve (Figure 6). However, we would like to caution that the periodic signal can not be robustly confirmed for the following reasons: (1) The source was not detected in many observations, and upper limits used in the test may introduce large uncertainty. (2) The confidence level of signals would be lower than the 99.9% with different assumptions of the noise (e.g. red noise). Future monitoring data are required to check the recurrence period.

3. DISCUSSION & CONCLUSIONS

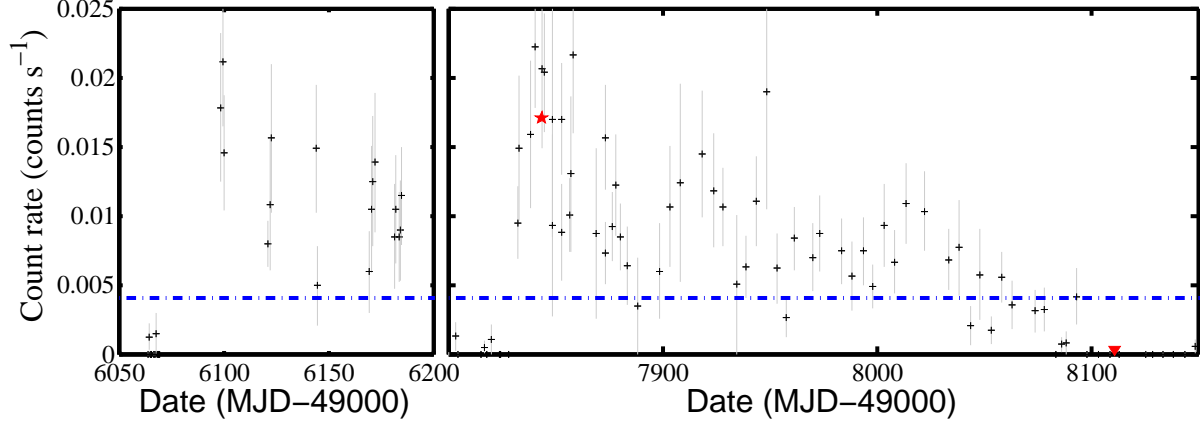


Figure 3. *Swift*/XRT count rate vs. MJD for two outbursts. The blue horizontal line mark the *Swift*/XRT threshold of 2σ detection with an exposure time of 1000 s. The red pentagram and downward-pointing triangle correspond to the detection and the 2σ upper limit derived from two *XMM-Newton* data (converted into XRT count rates).

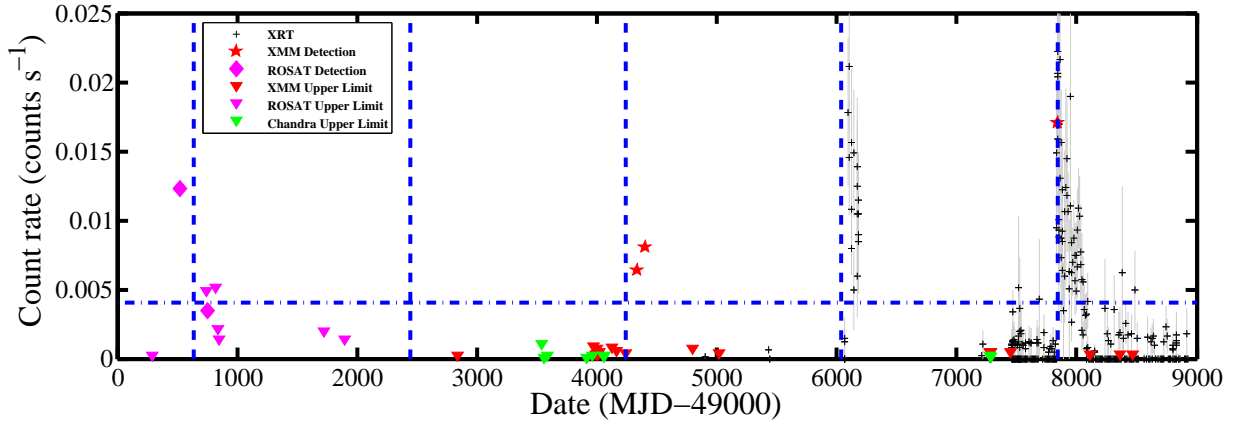


Figure 4. X-ray Light curve of 3XMM J031820.8-663034. Count rates and upper limits from other instruments were converted into *Swift*/XRT count rates. The blue horizontal line mark the *Swift*/XRT threshold of 2σ detection with an exposure time of 1000 s. The blue vertical lines spaced by 1800 days are plotted to better illustrate the quasi-periodic outbursts.

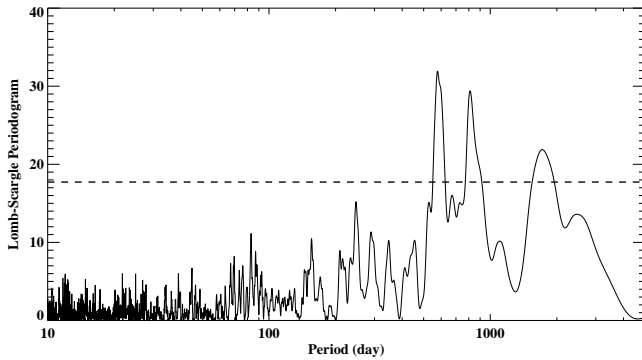


Figure 5. Lomb-Scargle periodogram for 3XMM J031820.8-663034. The dashed line indicates 99.9% significance.

In this work, we investigate the wealth of X-ray data of 3XMM J031820.8-663034 and reveal four periods of activities, making it as a transient ULX. The outburst properties are summarized as follows: (1) The outbursts likely occur regularly; (2) One outburst with sufficiently

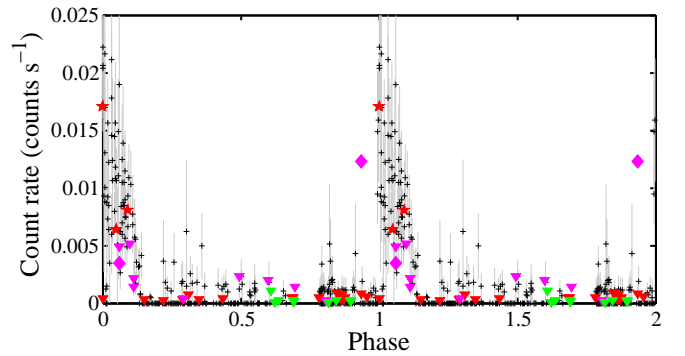


Figure 6. Folding the light curve in Figure 4 over a period of 1800 days.

dense sampling exhibits a fast rise slow decay profile; (3) The peak X-ray luminosity $L_{\text{peak}} \sim 1.5 \times 10^{39}$ erg/s does not change much among different outbursts; (4) The source occupies the thermal state at the high luminosity; (5) The deepest *Chandra* observation provides a luminosity upper limit of $\sim 5.6 \times 10^{36}$ erg/s for the quiescent state.

Table 3
Outburst parameters

	3XMM J031820.8-663034	HLX-1 [‡]
$T_{\text{recurrent}}$	~ 1800 days	~ 400 days
Duration	$\sim 240 - 300$ days	~ 113 days
Duty cycle	~ 0.15	~ 0.3
L_{peak}	$\sim 1.5 \times 10^{39}$ erg/s	$\sim 1.2 \times 10^{42}$ erg/s
Fluence [†]	$\sim 10^{46}$ erg	$\sim 5.8 \times 10^{48}$ erg
Amplitude	> 270	$\sim 20 - 50$

Note. — †: Averaged values are listed for HLX-1 (Godet et al. 2014; Yan et al. 2015). ‡: Fluence is referred to the total energy radiated during one outburst.

The evolving soft X-ray spectra from 3XMM J031820.8-663034 imply its accretion nature and the accreting object could be a black hole. High-mass X-ray binaries commonly consist of a neutron star and a young massive star, and have very hard X-ray spectra (e.g. Fabbiano 2006; Walter et al. 2015; Wang et al. 2016b). Thereby, the scenario of a canonical high-mass X-ray binary is disfavored for 3XMM J031820.8-663034. Because its peak luminosity marginally puts the source in the category of ULXs, below we compare its outburst properties with normal transient black hole binaries and other known transient ULXs including the intermediate-mass black hole candidate ESO 243-49 HLX-1.

3.1. Association with NGC 1313

Before discussing the nature of outbursts, we need to determine whether 3XMM J031820.8-663034 is associated with NGC 1313, or a foreground/background object. The high Galactic latitude ($l = 283.3634^\circ$ and $b = -44.6295^\circ$) indicates that the source is unlikely a foreground star. Moreover, if the source is at a distance of less than 10 kpc, its peak X-ray luminosity during the outbursts would be less than 10^{34} erg/s. The X-ray spectrum of such a very faint X-ray transient should be dominated by non-thermal component (e.g. McClintock & Remillard 2006; Weng & Zhang 2015; Wijnands et al. 2015), contradicting the *XMM-Newton* and *Swift* observations which are in favor of the thermal dominated spectra. We can therefore exclude the possibility of a Galactic counterpart.

Alternatively, we estimate the probability of background QSO/AGN using X-ray $\log N - \log S$ (e.g. Wang et al. 2016a). According to the new *XMM-Newton* detection, the source has an absorbed flux in 0.5–2 keV of 2.3×10^{-13} erg/cm²/s. We would expect ~ 0.5 contaminating source per square degree with the same or higher flux based on the Lockman Hole $\log N - \log S$ relation (Hasinger et al. 1998; Mushotzky et al. 2000; Moretti et al. 2003; Wang et al. 2016a). Meanwhile, the D_{25} isophote of NGC 1313 is about $\sim 9.1'$ (Liu & Bregman 2005), and the distance between 3XMM J031820.8-663034 and the center of NGC 1313 is $\sim 0.8'$. Therefore, the number of expected background sources within the D_{25} of NGC 1313 (or in $0.8'$) is only ~ 0.01 (or 9×10^{-5}). Furthermore, the chance that a background source has similar dramatic variations is even lower. We thus conclude the association of 3XMM J031820.8-663034 with NGC 1313 is convincing.

3.2. Repeated outbursts

A straightforward explanation for the regular outbursts is that the mass transfer rate is significantly enhanced during the periastron passage of the donor star bounded to the black hole in an eccentric orbit. However the formation of a black hole binary with such long period (~ 1800 days) could be challenging. To our knowledge, GRS 1915+105 has the longest orbital period (~ 33.5 days, Greiner et al. 2001) among LMXBs (Liu et al. 2007). Meanwhile, very few high-mass X-ray binaries have periods longer than 10^3 days (Liu et al. 2006), e.g. PSR B1259-63 (~ 3.4 years, Johnston et al. 1994) and PSR J2032+4127 ($\sim 25 - 50$ years, Lyne et al. 2015; Ho et al. 2017), both of which are faint in X-ray ($L_X < 10^{35}$ erg/s). On the other hand, during the early observations HLX-1 displayed regular outbursts at an interval of ~ 1 yr (Farrell et al. 2009a; Webb et al. 2012). However, the initial hypothesis that the recurrence time corresponded to the binary period became controversial due to the increasing of the detected recurrence time (Godet et al. 2014; Weng & Feng 2018).

In addition, the super-orbital periods have been reported in tens of X-ray binaries (Sood et al. 2007; Farrell et al. 2009b), and some of them could be more than 10^3 days (e.g. ~ 1667 days for LS I +61° 303, Li et al. 2012), similar to the recurrent time of 3XMM J031820.8-663034. However the amplitude of super-orbital modulation (e.g. Smith et al. 2007; Corbet & Krimm 2013) is significantly smaller than that of 3XMM J031820.8-663034 (> 270). Thus, whether the outbursts of 3XMM J031820.8-663034 are some kind of super-orbital modulation is still questionable.

Note a small number of LMXBs, e.g. 4U 1630-47 (Parmar 1995; Capitanio et al. 2015) and H1743-322 (Yan et al. 2015), exhibited some successive (not all) outbursts equally spaced in time. The light curve profiles of these outbursts could be complicated, but not always the typical “fast-rise exponential-decay”. It was suggested that the periodicity was resulted from the DIM, or sometimes with additional perturbation from the companion star mass transfer (Capitanio et al. 2015). Here, since only four outbursts are recorded for 3XMM J031820.8-663034 and the observation cadence is incomplete, we suggest that more monitoring data are required to check whether the quasi-periodic behaviors are temporary or represent some process in physics. As further discussed below, all available data at the current stage can be interpreted with the DIM.

3.3. Outburst mechanism

There are two transient ULXs detected in M31, i.e. CXOM31 J004253.1+411422 (Kaur et al. 2012; Middleton et al. 2012) and XMMU J004243.61+412519 (Middleton et al. 2013). Middleton et al. (2012) found the X-ray luminosity of CXOM31 J004253.1+411422 steadily declined from 5×10^{39} erg/s to 6×10^{38} erg/s over 1.5 month (see also Kaur et al. 2012). XMMU J004243.61+412519 entered an outburst in 2012 January, reached a peak X-ray luminosity of $\sim 1.26 \times 10^{39}$ erg/s within a few days, and then decayed slowly (Middleton et al. 2013). Their outburst parameters resemble those found in Galactic LMXBs, indicating a DIM origin for these two sources as well (e.g. Yan & Yu 2015). However only one outburst had been observed for

each source thus the recurrence timescale is unavailable.

It is worth to note that the recurrence outbursts of the best studied transient ULX, HLX-1, are analogous to the outbursts of 3XMM J031820.8-663034 in many aspects. Meanwhile, the outbursts of HLX-1 have significantly higher luminosity at both active and quiescent states, and smaller amplitude of luminosity variation. The total energy radiated during an outburst is about 2-3 orders of magnitude larger than the averaged value observed in 3XMM J031820.8-663034 (Table 3). Yan et al. (2015) argued that HLX-1 and LMXBs follow the same linear relationship between the hard-to-soft state transition luminosity and the peak luminosity, but the data of HLX-1 deviate the correlation between the X-ray fluence and peak luminosity observed in LMXBs (Figure 7). The minimum observed X-ray luminosity of HLX-1 is up to $\sim 3 \times 10^{40}$ erg/s, indicating that the thin disk within a very large radius ($\sim 10^{13}$ cm) is fully ionized because of large accretion rate and the additional heating by the strong irradiation (Dubus et al. 2001; Soria et al. 2017). In this case, the local thermal-viscous instability should be ignited (if existed) at even larger physical radius (not the black hole mass scaled radius). Such instability would take at least 100 years to reach the inner most accretion disc, which however contradicts the observed value of ~ 100 days (Lasota et al. 2011). Therefore, the HLX-1 outbursts are unlikely due to thermal-viscous instability (i.e. DIM) but might be attributed to the radiation pressure instability (Lasota et al. 2011; Sun et al. 2016) or other instabilities.

Investigating the optical/UV and X-ray data, Soria et al. (2017) proposed an oscillating wind scenario for HLX-1: currently its accretion rate is on average of a few percent Eddington and its accretion disk is quite large ($\sim 10^{13}$ cm); but only the inner region ($\leq 10^{12}$ cm) of the inflow is modulated by the wind instability (Begelman et al. 1983; Shields et al. 1986), which drives the outbursts at a timescale of ~ 1 yr. Such model might also work for V404 Cyg (Muñoz-Darias et al. 2016). Due to the limited data, we do not know whether the strong wind can be launched from 3XMM J031820.8-663034, and whether the wind instability model is applicable to its repeated outbursts. The model is presented here as an option. Alternatively, we argue that the outburst properties of 3XMM J031820.8-663034 reported in this paper can be understood in the framework of DIM.

The X-ray luminosity at the quiescent state of 3XMM J031820.8-663034 ($< 5.6 \times 10^{36}$ erg/s) indicates that the disk is cool due to a low accretion rate and weak irradiation. The partial hydrogen ionization instability (i.e. thermal-viscous instability) thus emerges at a much smaller radius and allows the DIM to work. Additionally, we point out that most of the outbursts properties are consistent with the expectation of DIM: (1) The light curve shows a fast rise slow decay profile. (2) It falls on the same relation between the outburst fluence and the peak luminosity that was found for LMXBs (Yan & Yu 2015). Such correlation is expected in DIM since the outburst peak increases with the mass of accretion disk (e.g. Dubus et al. 2001). Assuming a constant radiative efficiency, the mass of accretion disk and the peak accretion rate can be estimated from the fluence and the L_{peak} , respectively. (3) Taking the truncation and irradi-

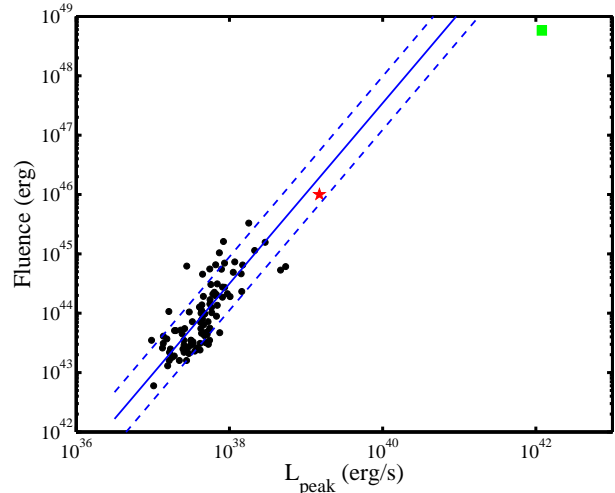


Figure 7. Total energy radiated during the outburst vs. peak X-ray luminosity. The filled circles correspond to the outbursts of LMXBs adopted from Yan & Yu (2015). The blue lines indicate the best-fit result with a linear model in a logarithmic scale (solid) and the 3σ confidence intervals (dashed). The red pentagram and the green square mark 3XMM J031820.8-663034 and HLX-1, respectively.

ation effects into account, theoretical DIM models yield the recurrence time of $1 \sim 180$ years (Dubus et al. 2001; Lasota 2001), conforming to that of 3XMM J031820.8-663034 (~ 1800 days).

In addition to X-ray, the nature of the outbursts can be explored with multi-wavelength data. The optical/UV data could provide key information of the companion star and the X-ray irradiated accretion disk (e.g. Rykoff et al. 2007; Weng & Zhang 2015; Soria et al. 2017). Furthermore, the connections between accretion flows and the radio jet have been widely studied (e.g. Fender et al. 2004; Zhang et al. 2014). A stable jet is commonly detected in the low/hard state, while the discrete ejection events are found to be associated with the transitions between the low/hard and the high/soft states. We search the radio images in the literature and the SkyView⁵, but do not find the point like source at the position of 3XMM J031820.8-663034 in the 1.4 GHz radio continuum map (Ryder et al. 1993) nor the SUMSS 843 MHz image. A detailed analysis on these data is beyond the purpose of this paper.

3.4. Accretion state & black hole mass

Most Galactic LMXBs are in the regime of sub-Eddington accretion with variable X-ray emission. Although different state classifications have been proposed by different authors (e.g. McClintock & Remillard 2006; Zhang 2013; Yuan & Narayan 2014), the low/hard and the high/soft states are normally undisputed. The low/hard state is characterized by a hard spectrum and strong rapid variations. In contrast, the high/soft state is dominated by a thermal disk component and has a low level of variability. Meanwhile, several Galactic LMXBs can occasionally be brighter than 10^{39} erg/s, e.g. GRS 1915+105 (e.g. Belloni et al. 2000; Yan et al. 2017), V4641 Sgr (Revnivtsev et al. 2002) and V404 Cyg

⁵ <https://skyview.gsfc.nasa.gov/current/cgi/query.pl>

(e.g. Motta et al. 2017, and references therein). These three sources are highly variable on time-scales of minutes to hours during the outbursts. In particular, during the 2015 outburst, V404 Cyg showed violent variations in both X-ray and optical bands (Kimura et al. 2016) and the non-thermal dominated X-ray emission (e.g. Sánchez-Fernández et al. 2017; Motta et al. 2017). The source did not enter into the canonical high/soft state, but might be accreting at super-Eddington accretion rate. Its evolution pattern is distinct from other typical LMXBs.

The new *XMM-Newton* detection of 3XMM J031820.8-663034 performed at the peak of an outburst indicates that its spectrum is dominated by a thermal disk component and no significant variation is detected within the XMM exposure. The X-ray properties are consistent with the definition of the high/soft state, that is, the source reaches a luminosity of $(0.1 - 1) L_{\text{Edd}}$ during the outbursts. Compared to those Galactic LMXBs at the high/soft state, 3XMM J031820.8-663034 has a higher peak X-ray luminosity ($\sim 1.5 \times 10^{39}$ erg/s), which might indicate a heavier black hole (tens of solar masses) hosted in the system. The MsBH scenario is also supported by the fitted disk black-body normalization ($\sim 0.02 - 0.03$, Arnaud 1996), which corresponds to a radius of ~ 300 km with a inclination angle of 60° and a spectral hardening factor of 1.7 adopted. If the accretion disk extends to the innermost stable circular orbit, the derived radius corresponds to $\sim 30 - 200 M_\odot$ for a Schwarzschild and a maximally rotating black hole, respectively.

We thank the anonymous referee for the helpful comments. We acknowledge the use of public data from the High Energy Astrophysics Science Archive Research Center Online Service. We thank Drs. Wei-Min Gu, Zhen-Yi Cai and C.-Y. Ng for many valuable discussions. This work is supported by the National Natural Science Foundation of China under grants 11703014, 11673013, 11421303, and 11573023, the Natural Science Foundation from Jiangsu Province of China (Grant No. BK20171028), and the University Science Research Project of Jiangsu Province (17KJB160002). J.X.W. thanks support from Chinese Top-notch Young Talents Program, and CAS Frontier Science Key Research Program QYCDJ-SSW-SLH006.

Facilities: *ROSAT*, *XMM-Newton*, *Chandra*, Neil Gehrels *Swift* Observatory.

Software: SAS, HEASOFT, CIAO.

REFERENCES

- Arnaud, K. A. 1996, in ASP Conf. Ser. 101, *Astronomical Data Analysis Software and Systems V*, ed. G. H. Jacoby & J. Barnes (San Francisco, CA: ASP), 17
- Bachetti, M., Rana, V., Walton, D. J., et al. 2013, *ApJ*, 778, 163
- Begelman, M. C., McKee, C. F., Shields, G. A., 1983, *ApJ*, 271, 70
- Belloni, T., Klein-Wolt, M., Méndez, M., van der Klis, M., & van Paradijs, J. 2000, *A&A*, 355, 271
- Capitanio, F., Campana, R., De Cesare, G., Ferrigno, C., 2015, *MNRAS*, 450, 3840
- Cash, W., 1979, *ApJ*, 228, 939
- Chen, W., Shrader, C. R., Livio, M. 1997, *ApJ*, 491, 312
- Corbet, R. H. D. & Krimm, H. A. 2013, *ApJ*, 778, 45
- Corral-Santana, J. M., Casares, J., Muñoz-Darias, T., et al. 2016, *A&A*, 587, 61
- Crivellari, E., Wolter, A., & Trinchieri, G. 2009, *A&A*, 501, 445
- Dubus, G., Hameury, J. M., Lasota, J. P., 2001, *A&A*, 373, 251
- Fabbiano, G. 2006, *ARA&A*, 44, 323
- Farrell, S. A., Barret, D., Skinner, G. K., 2009b, *MNRAS*, 393, 139
- Farrell, S. A., Webb, N. A., Barret, D., Godet, O., & Rodrigues, J. M. 2009a, *Natur*, 460, 73
- Fender, R. P., Belloni, T. M., & Gallo, E. 2004, *MNRAS*, 355, 1105
- Feng, H., & Soria, R. 2011, *New Astron. Rev.*, 55, 166
- Gao, Q., Wang, W., Liu, J.-F., & Yoachim, P. 2015, *ApJ*, 799, 19
- Gehrels, N., Chincarini, G., Giommi, P., et al. 2004, *ApJ*, 611, 1005
- Godet, O., Lombardi, J. C., Antonini, F., et al. 2014, *ApJ*, 793, 105
- Greiner, J., Cuby, J. G., & McCaughrean, M. J. 2001, *Natur*, 414, 522
- Grimm, H.-J., McDowell, J., Zezas, A., Kim, D.-W., & Fabbiano, G. 2007, *ApJS*, 173, 70
- Hasinger, G., Burg, R., Giacconi, R., et al. 1998, *A&A*, 329, 482
- Ho, W. C. G., Ng, C.-Y., Lyne, A. G., et al. 2017, *MNRAS*, 464, 1211
- Horne, J. H., & Baliunas, S. L. 1986, *ApJ*, 302, 757
- Johnston, S., Manchester, R. N., Lyne, A. G., Nicastro, L., Spyromilio, J., 1994, *MNRAS*, 268, 430
- Kaaret, P., Feng, H. & Roberts, T. P. 2017, *ARA&A*, 55, 303
- Kaur, A., Henze, M., Haberl, F., et al. 2012, *A&A*, 538, A49
- Kimura, M., Isogai, K., Kato, T., et al. 2016, *Nature*, 529, 54
- Kosec, P., Pinto, C., Fabian, A. C., & Walton, D. J., 2018, *MNRAS*, 473, 5680
- La Parola, V., DAi, A., Cusumano, G., & Mineo, T. 2015, *A&A*, 580, A71
- Lasota, J. P. 2001, *New Astron. Rev.*, 45, 449
- Lasota, J.-P., Alexander, T., Dubus, G., et al. 2011, *ApJ*, 735, 89
- Lasota, J.-P., King, A. R., & Dubus, G. 2015, *ApJL*, 801, L4
- Li, J., Torres, D. F., Zhang, S., et al. 2012, *ApJL*, 744, L13
- Lin, D., Webb, N. A., & Barret, D. 2014, *ApJ*, 780, 39
- Liu, J.-F., & Bregman, J. N. 2005, *ApJS*, 157, 59
- Liu, Q. Z., van Paradijs, J., & van den Heuvel, E. P. J. 2006, *A&A*, 455, 1165
- Liu, Q. Z., van Paradijs, J., & van den Heuvel, E. P. J. 2007, *A&A*, 469, 807
- Lyne, A. G., Stappers, B. W., Keith, M. J., Ray, P. S., Kerr, M., Camilo, F., Johnson, T. J., 2015, *MNRAS*, 451, 581
- Makishima, K., Kubota, A., Mizuno, T., et al. 2000, *ApJ*, 535, 632
- McClintock, J. E., & Remillard, R. A. 2006, in *Compact Stellar X-ray Sources*, eds. W.H.G. Lewin and M. van der Klis (Cambridge: Cambridge Univ. Press)
- Middleton, M. J., Sutton, A. D., Roberts, T. P., Jackson, F. E., & Done, C. 2012, *MNRAS*, 420, 2969
- Middleton, M. J., Miller-Jones, J. C. A., Markoff, S., et al. 2013, *Natur*, 493, 187
- Miller, M. C., Farrell, S. A., & Maccarone, T. J. 2014, *ApJ*, 788, 116
- Moretti, A., Campana, S., Lazzati, D., & Tagliaferri, G. 2003, *ApJ*, 588, 696
- Motta, S. E., Kajava, J. J. E., Sánchez-Fernández, C., et al. 2017, *MNRAS*, 471, 1797
- Mushotzky, R., Cowie, L., Barger, A., & Arnaud, K. 2000, *Nature*, 404, 459
- Muñoz-Darias, T., et al., 2016, *Nature*, 534, 74
- Parmar, A. N., Angelini, L., White, N. E., 1995, *ApJL*, 452, L29
- Petre, R., Okada, K., Mihara, T., Makishima, K., & Colbert, E. J. M. 1994, *PASJ*, 46, L115
- Pfeffermann, E., Briel, U. G., Hippmann, H., et al. 1987, *Proc. SPIE*, 733, 519
- Pinto, C., Middleton, M. J., & Fabian, A. C. 2016, *Nature*, 533, 64
- Reig, P., 2011, *Ap&SS*, 332, 1
- Revnivtsev, M., Gilfanov, M., Churazov, E., Sunyaev, R., 2002, *A&A*, 391, 1013
- Ryder, S., Staveley-Smith, L., Dopita, M., Petre, R., Colbert, E., Malin, D., & Schlegel, E. 1993, *ApJ*, 416, 167
- Rykoff, E. S., Miller, J. M., Steeghs, D., & Torres, M. A. P. 2007, *ApJ*, 666, 1129

- Sánchez-Fernández, C., Kajava, J. J. E., Motta, S. E., & Kuulkers, E., 2017, *A&A*, 602, A40
- Shields, G. A., McKee, C. F., Lin, D. N. C., Begelman, M. C., 1986, *ApJ*, 306, 90
- Smith, D. M., Heindl, W. A., & Swank, J. H. 2002, *ApJL*, 578, L129
- Sood, R., Farrell, S., O'Neill, P., & Dieters, S. 2007, *Advances in Space Research*, 40, 1528
- Soria, R., Musaeva, A., Wu, K., et al. 2017, *MNRAS*, 469, 886
- Strüder L. et al., 2001, *A&A*, 365, L18
- Sun, M., Gu, W.-M., Yan, Z., Wu, Q.-W., & Liu, T. 2016, *MNRAS*, 463, 99
- Truemper, J. 1982, *AdSpR*, 2, 241
- Turner M. J. L. et al., 2001, *A&A*, 365, L27
- VanderPlas, J. T. 2017, *arXiv:1703.09824*
- Walter, R., Lutovinov, A. A., Bozzo, E., & Tsygankov, S. S. 2015, *A&A Rev.*, 23, 2
- Wang, S., Liu, J.-F., Qiu, Y.-L., et al. 2016b, *ApJS*, 224, 40
- Wang, S., Qiu, Y.-L., Liu, J.-F. & Bregman, J. N. 2016a, *ApJ*, 829, 20
- Webb, N., Cseh, D., Lenc, E., et al. 2012, *Sci*, 337, 554
- Weisskopf, M. C., Tananbaum, H. D., Van Speybroeck, L. P., & O'Dell, S. L. 2000, *Proc. SPIE*, 4012, 2
- Weng, S.-S., & Feng, H. 2018, *ApJ*, 853, 115
- Weng, S.-S., Wang, J.-X., Gu, W.-M., & Lu, J.-F. 2009, *PASJ*, 61, 1287
- Weng, S.-S., Zhang, S.-N., & Zhao, H.-H. 2014, *ApJ*, 780, 147
- Weng, S.-S., & Zhang, S.-N. 2015, *MNRAS*, 447, 486
- Wijnands, R., Degenaar, N., Armas Padilla, M., et al. 2015, *MNRAS*, 454, 1371
- Yan, Z., & Yu, W. 2015, *ApJ*, 805, 87
- Yan, Z., Zhang, W., Soria, R., Altamirano, D., & Yu, W. 2015, *ApJ*, 811, 23
- Yan, S.-P., Ji, L., Méndez, M., Liu, S.-M., Wang, N. et al. 2017, *MNRAS*, 465, 1926
- Yuan, F., & Narayan, R. 2014, *ARA&A*, 52, 529
- Zezas, A., Fabbiano, G., Baldi, A., et al. 2006, *ApJS*, 166, 211
- Zhang, J.-F., Xu B., Lu J.-F., 2014, *ApJ*, 788, 143
- Zhang, S.-N. 2013, *FrPhy*, 8, 630
- Zhao, H.-H., Weng, S.-S., & Ng, C.-Y. 2017, *MNRAS*, 468, 1551